Review of Scientific Instruments

Quantitative scanning thermal microscopy based on determination of thermal probe dynamic resistance

Cite as: Rev. Sci. Instrum. **84**, 093702 (2013); https://doi.org/10.1063/1.4819738
Submitted: 16 April 2013 • Accepted: 15 August 2013 • Published Online: 09 September 2013

J. Bodzenta, J. Juszczyk and M. Chirtoc

Quantitative scanning thermal microscopy based on determination of thermal probe dynamic resistance

J. Bodzenta,[1,a)] J. Juszczyk,[1] and M. Chirtoc[2]
[1]*Institute of Physics, Silesian University of Technology, 44-100 Gliwice, Poland*
[2]*Multiscale Thermophysics Lab GRESPI-CATHERM, Université de Reims Champagne-Ardenne URCA, Moulin de la Housse, BP 1039, 51687 Reims, France*

(Received 16 April 2013; accepted 15 August 2013; published online 9 September 2013)

Resistive thermal probes used in scanning thermal microscopy provide high spatial resolution of measurement accompanied with high sensitivity to temperature changes. At the same time their sensitivity to variations of thermal conductivity of a sample is relatively low. In typical dc operation mode the static resistance of the thermal probe is measured. It is shown both analytically and experimentally that the sensitivity of measurement can be improved by a factor of three by measuring the dynamic resistance of a dc biased probe superimposed with small ac current. The dynamic resistance can be treated as a complex value. Its amplitude represents the slope of the static voltage-current *U-I* characteristic for a given *I* while its phase describes the delay between the measured ac voltage and applied ac current component in the probe. The phase signal also reveals dependence on the sample thermal conductivity. Signal changes are relatively small but very repeatable. In contrast, the difference between dynamic and static resistance has higher sensitivity (the same maximum value as that of the 2nd and 3rd harmonics), and also much higher amplitude than higher harmonics. The proposed dc + ac excitation scheme combines the benefits of dc excitation (mechanical stability of probe-sample contact, average temperature control) with those of ac excitation (base-line stability, rejection of ambient temperature influence, high sensitivity, lock-in signal processing), when the experimental conditions prohibit large ac excitation. © *2013 AIP Publishing LLC*. [http://dx.doi.org/10.1063/1.4819738]

I. INTRODUCTION

Scanning thermal microscopy (SThM) developed by Williams and Wickramasinghe[1,2] is a variant of atomic force microscopy (AFM) in which temperature sensitive probes are used. It allows obtaining topographic and thermal images of a sample simultaneously. Two types of thermal images can be recorded. In passive mode the thermal probe (TP) measures local temperature at the surface of a sample. Such measurement allows for mapping temperature distribution of self-heated structures[3,4] and devices.[5,6] In active mode the TP heats the sample and the probe temperature is measured. This temperature depends on heating power and heat losses which include heat flux from the TP to the sample. Among other things, the heat flux depends on the thermal conductivity κ of the sample, therefore the TP temperature carries information about κ of the sample in the vicinity of probe-sample contact. In active mode spatial distribution of κ at the sample surface can be obtained.[7]

Despite the fact that SThM has been in development for more than 25 years there are still problems without satisfactory solutions. One of them is quantitative κ measurement by commercial SThM equipment. In the majority of papers published on this topic measurement with Wollaston wire resistive probe was considered. The theoretical model of the probe-sample system, based on the transient fin equation including a source term due to the Joule dissipation, is well-established.[8–10] Its counterpart for nanofabricated TP has been also proposed.[11] The nanofabricated TP is a thin dielectric cantilever with bent, triangular end forming the probe tip. A thin film metallic resistor, playing a role of resistive thermometer and heater, is deposited near the tip apex. There are a few types of experiments in which TPs are used for quantitative measurement. The simplest one is based on dc measurement.[12,13] Although details of particular experiments can differ, the basic idea is the same. The probe-sample contact opens an additional channel for heat abstraction from the TP. In constant current mode, it lowers probe temperature and resistance. In constant temperature mode, the heating power must be increased to compensate for the heat loss. This technique was used for thermal conductivity measurements on several examples, e.g., meso-porous silicon thin films,[14] Bi_2Te_3 and Bi_2Se_3 thin films,[15] and pure titanium.[16] The dc experiments are simple but sensitive to noise. To improve signal to noise ratio ac measurements with lock-in detection are chosen. The basic idea of this group of methods is similar to the one of the 3ω method.[17] Nonlinearity of the TP causes generation of higher harmonics of voltage when the ac current flows through it. However, proper interpretation of measured signals is different than in the case of "classical" 3ω measurement.[9] Two regions can be distinguished in the spectral characterization of the signal.[18] At low frequencies, the isothermal region, signal amplitude depends on κ of the sample. At high frequencies, the adiabatic region, signal amplitude is considerably lower and does not depend on sample properties. Weak dependence of signal phase on the sample κ is observed in the transition region. The

a)Author to whom correspondence should be addressed. Electronic mail: Jerzy.Bodzenta@polsl.pl

capability of this measuring technique was proved in investigation of silicon nanowires embedded in a silica matrix[11] and NiTi samples.[19,20]

As it was mentioned above, when TPs are used in experiments with 3ω detection they must operate in the isothermal region to have sensitivity to the thermal properties of a sample. This does not present problems in the case of relatively massive Wollaston wire TPs. However, in the case of nanofabricated TPs probe heating is accompanied with probe bending caused by thermal stresses. When the probe is heated by ac current at frequency ω the bending occurs at frequency 2ω, the frequency of the heat source. According to the probes' specifications the resonance frequency of nanofabricated TPs is of about 50 kHz. It means that in the isothermal region, with upper limit of about 10 kHz (the frequency of the ac current), the probe bending keeps up periodic changes of dissipated power. The probe bending makes measurement difficult. There are problems with approaching the sample, keeping probe-sample contact, and assuring constant pressing force of the probe. It may cause loss of contact during measurement and even probe damage. In addition, the lock-in amplifier needs considerably longer time constants to measure higher harmonics than for the 1st harmonic. This is detrimental to 3ω detection in thermal imaging – the thermal image is shifted in relation to topographic image. These facts motivated us to propose a new way of performing experiments, which combines merits of both dc and ac excitation schemes. In Secs. II–IV we show that such an approach allows for avoiding the problems mentioned above with preservation of the benefits of dc and ac excitations.

II. UNDERLYING PRINCIPLE

The operation of resistive TPs is based on the dependence of the electrical resistivity ρ of metals on the temperature T. If considered temperature range is not very wide, this dependence is approximately linear:

$$\rho(T) = \rho_0 [1 + \alpha (T - T_0)], \tag{1}$$

where ρ_0 is the electrical resistivity at the temperature T_0 and α is its temperature coefficient. When the TP is driven by electric current, the Joule heating causes probe temperature rise and leads to nonlinearity of voltage-current dependence $U(I)$. Exemplary $U(I)$ dependencies measured for nanofabricated TP in air and the TP touching SiC surface are shown in Fig. 1. The solid straight line corresponds to the dependence calculated for a fixed 462 Ω resistor. Experimental data were fitted with cubic curves (dashed lines) resulting from Eq. (1) and given by

$$U = R_0 I + A I^3, \tag{2}$$

where I is the probe current, R_0 is the probe resistance at ambient temperature ($R_0 = 462$ Ω in analyzed case), and A is the nonlinearity coefficient, $A = 8.56 \pm 0.05$ Ω mA^{-2} and $A = 5.42 \pm 0.14$ Ω mA^{-2} for the probe in air and the probe touching SiC sample, respectively. Such form of $U(I)$ dependence for the probe is justified by the fact that in Eq. (1) the difference $(T - T_0)$ is proportional to the power dissipated in the probe by the current, which is proportional to I^2. Obtained

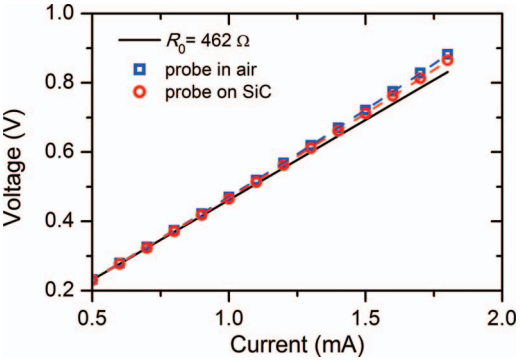

FIG. 1. Voltage-current characteristics measured for nanofabricated TP in air (□) and for the probe touching SiC (◯).Dotted lines are fits with Eq. (2) to experimental data. The solid straight line is the characteristic calculated for a fixed 462 Ω resistor.

A values show that the nonlinearity of U-I characteristic depends on the effectiveness of heat abstraction form the probe and it diminishes with growing heat exchange rate.

Quantitative measurements require selection of parameter or parameters of the measuring system and establishing their relation with the parameters of the sample. In SThM with resistive TPs measured signal is typically correlated with the probe resistance. Using the approximation of Eq. (2), the static resistance of the probe is

$$R = \frac{U}{I} = R_0 + A I^2. \tag{3}$$

Based on the data features above and with $I = 2.0$ mA, the resistance change (relative to the TP in air) due to contact with SiC sample is $\Delta R = 12.6$ Ω, which is 2.7% of R_0. Taking into account that SiC is a good thermal conductor, it can be stated that the sensitivity of the probe to κ of the sample is rather low.

Alternatively, the dynamic resistance R_d for each point can be defined as

$$R_\mathrm{d} = \frac{dU}{dI}. \tag{4}$$

Using the same approximation of Eq. (2), one gets

$$R_\mathrm{d} = R_0 + 3 A I^2. \tag{5}$$

Thus, the dynamic resistance is 3 times more sensitive to the system nonlinearity than the static one. R_d can be determined experimentally by driving the examined element (e.g., the TP) with a sum of dc current and small ac current superimposed on it:

$$I = I_\mathrm{dc} + I_\mathrm{ac} \cos(\omega t), \tag{6}$$

and measuring the corresponding amplitude U_ac of the ac component of probe voltage at frequency ω. If the condition $I_\mathrm{ac} \ll I_\mathrm{dc}$ is fulfilled, R_d of the element at the current I_dc is

$$R_d \approx \frac{U_\mathrm{ac}}{I_\mathrm{ac}}. \tag{7}$$

The above consideration presents the general idea of enhancing κ sensitivity of SThM by combining dc bias with advantages of modulated experiments. More detailed analysis

can be done in a frame of the model proposed by Dames and Chen.[21]

III. THEORY

The problem of using a resistive element simultaneously as heater and thermometer in experiments aiming at determination of thermal conductivity was considered in Ref. 21. If the electric current I flows through the resistance R it causes heat dissipation. The power of the heat source is

$$Q = RI^2 \approx R_0 I\,(t)^2\,. \tag{8}$$

The last approximation is justified due to small relative change of the probe resistance caused by heating (of about a few percent, see Sec. II).

In the considered case the electric current consists of dc and ac components (Eq. (6)) and then from Eq. (2) the voltage across the probe has a dc component and 3 harmonics:

$$U = U_{\rm dc} + \sum_{n=1}^{3} U_n\,(\omega)\cos\,(n\omega t + \varphi_n). \tag{9}$$

The 1ω, 2ω, and 3ω voltage components in frequency domain, determined experimentally by the use of lock-in amplifier, are described by the equation,[21]

$$U_{n\omega,\rm rms} = 2\alpha R_0^2 I_{\rm ac,rms}^3 Z_n\,(\eta,\,\omega)\,, \tag{10}$$

where $Z_n(\eta,\omega)$ is the complex transfer function for the nth harmonic and $\eta = I_{\rm dc}/I_{\rm ac}$. Exact form of Z_n depends on the thermal transfer function of the analyzed system $Z_{\rm th}$. This function describes a relation between the heating power and the temperature of the resistive element. In the frequency domain

$$\theta_\omega = T_\omega - T_0 = Q_\omega Z_{\rm th}. \tag{11}$$

General relations between $Z_n(\eta,\omega)$ and $Z_{\rm th}$ can be found in Ref. 21.

Let us restrict further considerations to TPs used in SThM. The Wollaston TPs were successfully modeled by the lumped approximation of suspended wire.[10,18] In this approximation,

$$Z_{\rm th} = \frac{R_{\rm th}}{1 + j\omega\tau}, \tag{12}$$

where $\tau = R_{\rm th}C_{\rm th}$, $R_{\rm th}$ is an effective thermal resistance to heat transfer from the TP to surroundings, $C_{\rm th}$ is an effective heat capacity of the probe-sample system, and $j = \sqrt{-1}$. There is a small discrepancy between this model and experimental results observed for nanofabricated TPs below the cut-off frequency,[11] nevertheless it can be used as the first approximation in this case, too.

Based on the general formulas from Ref. 20 we obtained equations for all components of the probe voltage:

$$U_{\rm dc} = \sqrt{2}\eta U_{0,\rm rms}\left[1 + \frac{\alpha P_{0,\rm dc} R_{\rm th}}{\eta^2}\left(\eta^2 + \frac{1}{2} + \frac{1}{1+\omega^2\tau^2}\right)\right], \tag{13}$$

$$U_{1,\rm rms} = U_{0,\rm rms}\left[1 + \frac{\alpha P_{0,\rm dc} R_{\rm th}}{\eta^2}\left(\eta^2 + \frac{1}{2} + \frac{2\eta^2}{1+j\omega\tau} + \frac{1}{4\,(1+2j\omega\tau)}\right)\right], \tag{14}$$

$$U_{2,\rm rms} = -j\frac{\alpha P_{0,\rm dc} R_{\rm th} U_{0,\rm rms}}{2\eta}\left(\frac{2}{1+j\omega\tau} + \frac{1}{1+2j\omega\tau}\right), \tag{15}$$

$$U_{3,\rm rms} = -\frac{\alpha P_{0,\rm dc} R_{\rm th} U_{0,\rm rms}}{4\eta^2\,(1+2j\omega\tau)}, \tag{16}$$

where $U_{0,\rm rms} = R_0 I_{\rm ac}/\sqrt{2}$ is the root-mean square (rms) value of ac voltage related to the current I flowing through the constant resistor R_0, and $P_{0,\rm dc} = R_0 I_{\rm dc}^2$ is the power dissipated by the dc component of this current in the same resistor.

Calculated dependencies of $U_{\rm dc}$, rms amplitudes and phases of all harmonics on $\omega\tau$ product are shown in Fig. 2. $U_{\rm dc}$ and $U_{n,\rm rms}$ were normalized to $U_{0,\rm rms}$. Calculations were carried out for $\alpha P_{0,\rm dc} R_{\rm th} = 0.1$ (estimated from experimental data shown in Fig. 1) and $\eta = 20$. A few basic conclusions can be drawn from analysis of Fig. 2. The amplitude of harmonics drops by about two orders of magnitude for each consecutive one. $U_{\rm dc}$ is practically frequency independent, $U_{1,\rm rms}$ shows small drop near $\omega\tau = 1$ (inset graph in Fig. 2(a)), while $U_{2,\rm rms}$ and $U_{3,\rm rms}$ exhibit dependencies typical for low-pass filters. The phase of the 1st harmonic exhibits weak frequency dependence near $\omega\tau = 1$. A closer look reveals a minimum (inset graph in Fig. 2(b)). Phases of the 2nd and the 3rd harmonics show frequency dependence typical for low-pass filters.

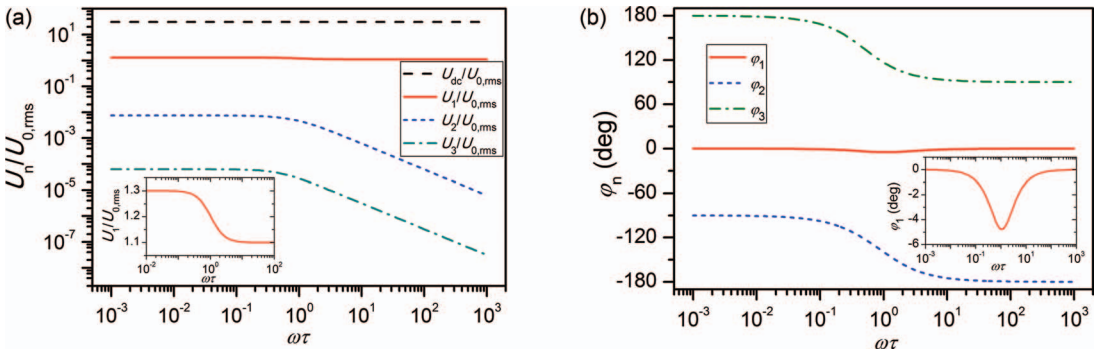

FIG. 2. Normalized amplitudes and phases of probe voltage components calculated for $\alpha P_{0,\rm dc} R_{\rm th} = 0.1$ and $\eta = 20$. In the case of harmonics it was assumed that the complex signal can be presented through its amplitude and phase, i.e., $U_{n,\rm rms} = U_n \exp(j\varphi_n)$.

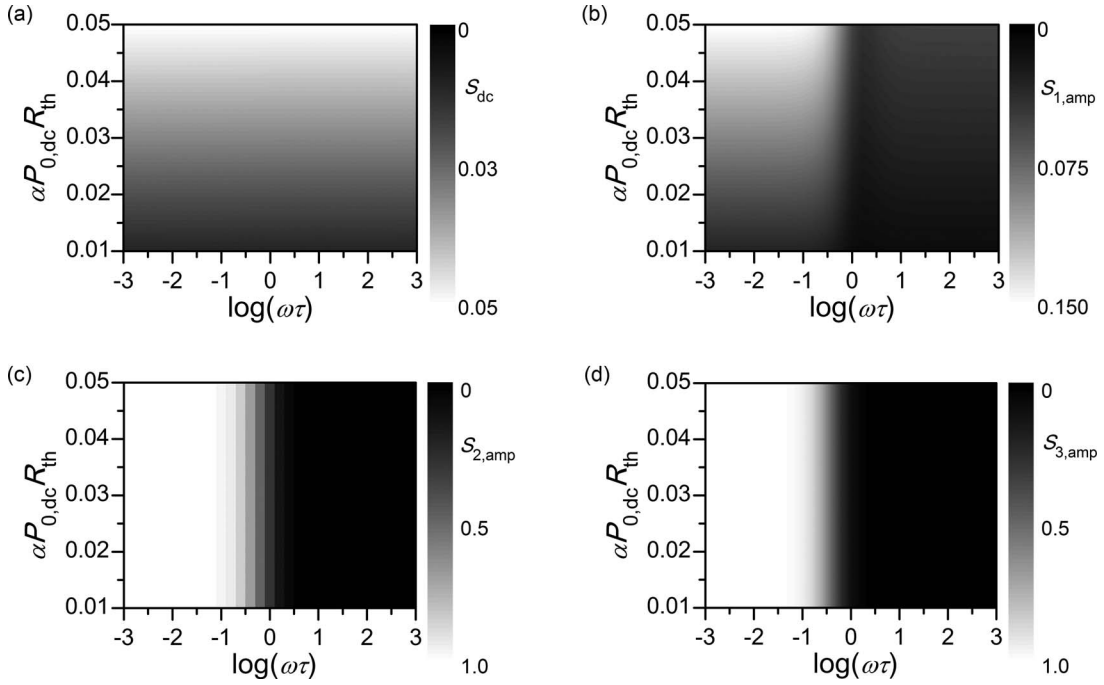

FIG. 3. Normalized sensitivities to R_{th} of dc component (S_{dc} – a) and of the amplitudes of ac signal components ($S_{1,amp}$ – b, $S_{2,amp}$ – c, $S_{3,amp}$ – d) as functions of dimensionless parameters $\omega\tau$ and $\alpha P_{0,dc} R_{th}$ (containing the effect of the sample), for $\eta = 20$.

To prove the usefulness of the proposed measuring procedure in SThM experiments a sensitivity of measured signal to changes of the effective thermal resistance has to be analyzed. This sensitivity can be defined as a normalized derivative of measured signal on R_{th}. For the dc signal and harmonics' amplitudes the normalized sensitivity was calculated based on the formula:

$$S_{dc/n,amp} = \frac{R_{th}}{\lim\limits_{\omega\tau\to 0} |U_{dc/n,amp}|} \frac{d(|U_{dc/n,amp}|)}{dR_{th}}, \tag{17}$$

while the phase sensitivity was defined as

$$S_{n,phase} = R_{th} \frac{d(\text{atan}(\text{Im}[U_{n,rms}]/\text{Re}[U_{n,rms}]))}{dR_{th}}. \tag{18}$$

Results obtained for the dc component and for the amplitudes of all harmonics are shown in Fig. 3.

It can be seen that dc and 1st harmonic "amplitude" sensitivities increase with increasing $\alpha P_{0,dc} R_{th}$. The dc component sensitivity S_{dc} is practically insensitive to $\omega\tau$, detailed analysis exhibits small sensitivity drop of about 0.4% near $\omega\tau \approx 1$. The sensitivity of 1ω component $S_{1,amp}$ is approximately three times higher than S_{dc} at low frequencies ($\omega\tau \ll 1$) and drops to the value of S_{dc} at higher frequencies ($\omega\tau \gg 1$). The sensitivities of 2ω and 3ω components are practically equal to one at low frequencies, drop to zero above $\omega\tau \approx 1$ and they are much higher than S_{dc} and $S_{1,amp}$. Such result can be expected as generation of higher harmonics is proportional to R_{th} (see Eqs. (15) and (16)). The practical problem is that accuracy of the amplitude determination of low signals is also low. In our case, $U_{1,rms}/U_{2,rms} = 133$ and $U_{1,rms}/U_{3,rms} = 16\,000$ at $\omega\tau \ll 1$. Therefore experiments based on determination of 2nd and 3rd harmonics could be difficult to perform with small ac excitation.

The analysis of phase sensitivities shows that the highest phase sensitivity can be expected in a vicinity of $\omega\tau = 1.0$ and that it is negative – the phase decreases with increasing R_{th} (Fig. 4). The phase sensitivity of the 1st harmonic is relatively low and $\alpha P_{0,dc} R_{th}$ dependent. It is also interesting that this sensitivity changes its sign for $\omega\tau \gg 1$ and becomes positive. The phase sensitivities of the 2nd and the 3rd harmonics are the highest in the vicinity of $\omega\tau = 1.0$, and the maximum sensitivity of the 2nd harmonic is observed at lower frequencies than the one of the 3rd harmonic. It should be also noticed that the phase sensitivities of higher harmonics are 10 times higher than the phase sensitivity of the fundamental one. Phase sensitivity peaks are rather sharp, therefore these sensitivities are strongly frequency dependent. From the practical point of view phase measurements for higher harmonics could be difficult because of their low amplitudes, as mentioned above.

Based on Eqs. (13) and (14) we can find formulas for the static and the dynamic resistances, which can be determined experimentally:

$$R_s = \frac{U_{dc}}{I_{dc}} = R_0 \left[1 + \frac{\alpha P_{0,dc} R_{th}}{\eta^2} \left(\eta^2 + \frac{1}{2} + \frac{1}{1+\omega^2\tau^2}\right)\right], \tag{19}$$

$$R_d = \frac{\sqrt{2}U_{1,rms}}{I_{ac}} = R_0 \left[1 + \frac{\alpha P_{0,dc} R_{th}}{\eta^2} \left(\eta^2 + \frac{1}{2} + \frac{2\eta^2}{1+j\omega\tau} + \frac{1}{4(1+2j\omega\tau)}\right)\right]. \tag{20}$$

At low frequencies ($\omega\tau \ll 1$), the exact sensitivity enhancement for $\eta = 20$ is thus $(R_d - R_0)/(R_s - R_0) = 2.99$ instead of 3.00 as estimated in Sec. II.

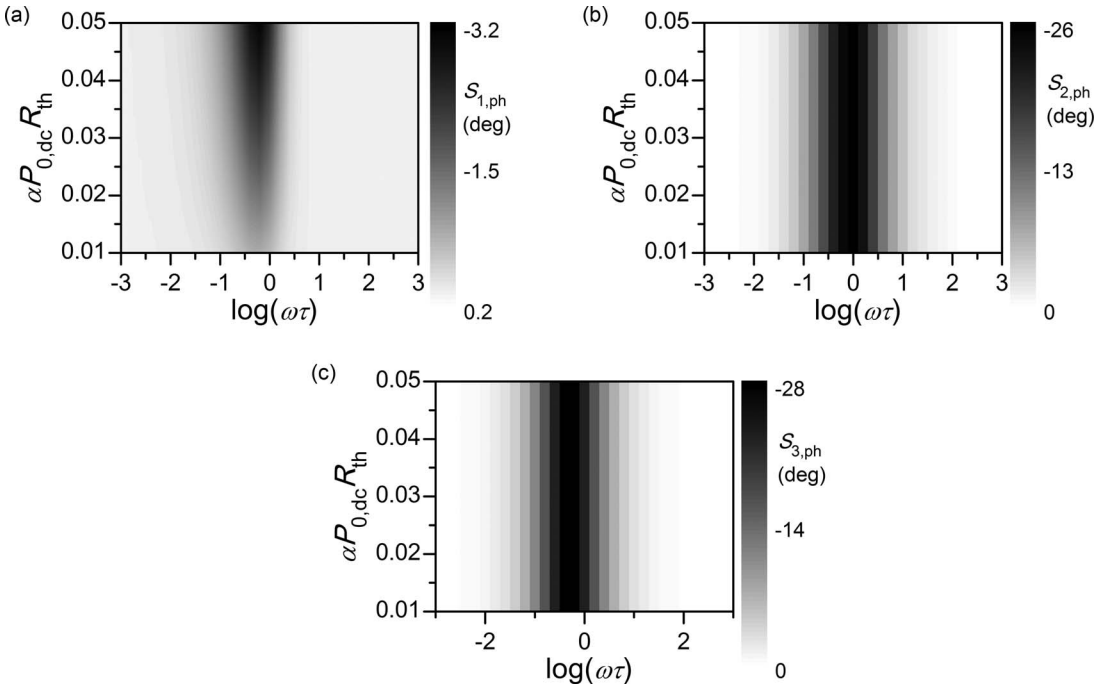

FIG. 4. Sensitivities to R_{th} of the phase of ac signal components ($S_{1,ph}$ – a, $S_{2,ph}$ – b, $S_{3,ph}$ – c) as functions of dimensionless parameters $\omega\tau$ and $\alpha P_{0,dc} R_{th}$ (containing the effect of the sample), for $\eta = 20$.

Since the highest sensitivities are found in the isothermal mode at low frequencies ($\omega\tau \ll 1$), this condition represents a useful special case for Eqs. (13)–(16). The resulting equations are equivalent to the ones derived in Ref. 10. Moreover, if the dc component is much larger than the ac one ($\eta \gg 1$), Eqs. (13)–(16) reduce to

$$U_{dc}^{n} = 1 + \alpha P_{0,dc} R_{th}, \tag{21}$$

$$U_{1}^{n} = 1 + 3\alpha P_{0,dc} R_{th}, \tag{22}$$

$$U_{2}^{n} = -j\frac{3}{2\eta}\alpha P_{0,dc} R_{th}, \tag{23}$$

$$U_{3}^{n} = -\frac{1}{4\eta^2}\alpha P_{0,dc} R_{th}. \tag{24}$$

Here U_{dc}^{n} and $U_{1,2,3}^{n}$ are the voltage components of Eqs. (13)–(16) normalized to $R_0 I_{dc}$ and $R_0 I_{ac}/\sqrt{2}$, respectively. Under the same conditions and from Eqs. (1), (11), and (12) $\alpha P_{0,dc} R_{th} \approx \Delta R/R_0$. This expression shows the direct link between the parameter of interest R_{th} and the relative variation of probe resistance $\Delta R/R_0$ which generates the voltage components of Eqs. (21)–(24). An alternate set of equations can be obtained by replacing the latter quantity in Eqs. (21)–(24).

IV. EXPERIMENTAL RESULTS

A diagram of the experimental setup is shown in Fig. 5. The voltage divider consisting of the TP and balance resistor R_b ($R_b \gg R_0$) was connected to the output of an Arbitrary Waveform Generator (Hewlett-Packard 33120 A). The dc current through the divider was measured by a digital multimeter (Agilent 34405 A). The probe voltage was passed to the input of a lock-in amplifier (SR 830 DSP, Stanford Research), connected in parallel with its analog-to-digital converter input. It allowed measurement of dc and selected ac components of the probe voltage. The TP was mounted in a probe holder of the atomic force microscope (XE-70, Park Inc.). Output signals from the lock-in could be used as external signal for the microscope for thermal imaging. The whole setup was controlled by PC with LabVIEW platform installed. Measuring procedure written in LabVIEW allowed measurement of U_{dc}, amplitudes and phases of $U_{1,rms}$, $U_{2,rms}$, and $U_{3,rms}$ as functions of I_{dc} and $f = \omega/2\pi$. All experiments were performed for $\eta = 20$.

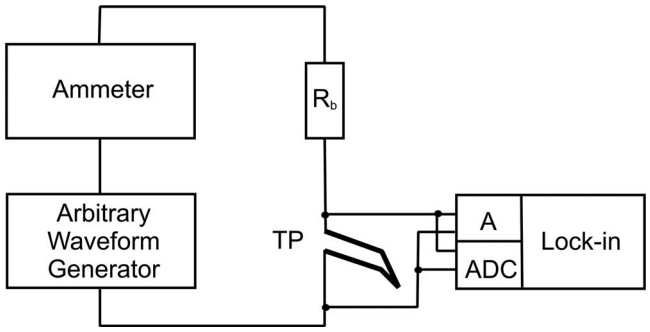

FIG. 5. Block diagram of the experimental setup. The current through the TP, connected in series with balance resistor R_b, was controlled by the signal from arbitrary waveform generator. The dc component of the current was measured by the ammeter. Lock-in amplifier measured dc and ac components of the TP voltage.

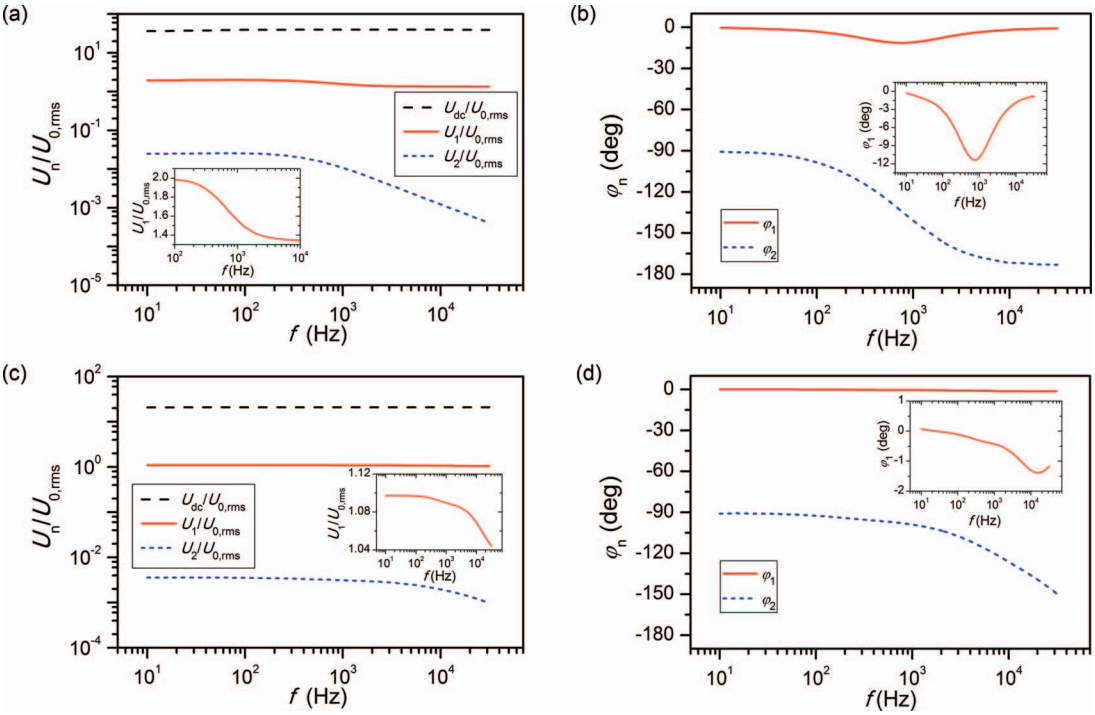

FIG. 6. Normalized amplitudes and phases of dc, 1st and 2nd voltage components of the Wollaston probe driven by 75 mA dc current with superimposed ac current of 3.7 mA amplitude (a) and (b) and the nanofabricated TP driven by 1.80 mA dc current with superimposed ac current of 0.09 mA amplitude (c) and (d). Behavior of the 1st harmonic near the cut-off frequency is depicted in inset graphs.

Experiments described in this paper were carried out using Wollaston wire probe and KNT-SThM-1an thermal probes (Kelvin Nanotechnology). The Wollaston wire probe was used for checking correctness of the theoretical model of measurement. Nanofabricated TPs were used in experiments the aim of which was to show the potentiality of proposed technique for qualitative and quantitative measurements.

The dc probe voltage and amplitudes and phases of the 1st and 2nd harmonics from the dc + ac biased Wollaston and nanothermal probes are shown in Fig. 6. The voltage signals were normalized to the 1st harmonic measured on unbiased probe ($I_{dc} = 0$). The 3rd harmonic signal was very low and its amplitude and phase could not be measured with satisfying accuracy. The behavior of all shown signals is very similar to the one predicted theoretically (Fig. 2). The cut-off frequency of the Wollaston probe is estimated to be of about 600 Hz, while the one of the nanofabricated probe is of about 10 kHz. The amplitude of $U_{2,rms}$ is more than 2 orders of magnitude lower than the one of $U_{1,rms}$. A characteristic minimum in the phase of the 1st harmonic can be seen near the cut-off frequency. Presented results allow concluding that the lumped approximation of suspended wire describes well the Wollaston probe driven by combined dc + ac bias current. In the case of the nanofabricated TP some discrepancies between this model and the experimental data can be noticed at frequencies preceding the cut-off frequency. Nevertheless qualitative agreement between the model and experimental results seems to be still acceptable.

The main goal of this work was to demonstrate the advantages of using dc biased ac driven TPs in quantitative thermal measurements. We know from experience that there are a few factors accomplishing the quantitative thermal measurements with SThM. The main one is that the probe-sample heat flux constitutes only a small part of the heat flux from the sample to surroundings. Therefore the method should be very sensitive to small changes of R_{th}. However, there are also practical aspects that must be taken into account when designing experiment. The formulas for signals which can be determined experimentally (Eqs. (13)–(16)) contain $U_{0,rms}$ and $P_{0,dc}$, both depending on R_0 which is affected by ambient temperature drift. It would be preferable to have a reference signal allowing proper signal correction. The simplest solution is to measure the signal for the TP in contact with the sample and in air. From Eqs. (19) and (20), the difference between R_d and R_s in each case is

$$R_d - R_s = \frac{\alpha P_{0,dc} R_0}{\eta^2} R_{th} \times \left(\frac{2\eta^2}{1 + j\omega\tau} + \frac{1}{4(1+2j\omega\tau)} - \frac{1}{1+\omega^2\tau^2} \right). \quad (25)$$

At low frequencies ($\omega\tau \ll 1$) the ratio of these differences obtained "in contact" and "out of contact" is equal to the ratio of the effective thermal resistances in both cases,

$$\frac{(R_d - R_s)_{in}}{(R_d - R_s)_{out}} = \frac{R_{th}|_{in}}{R_{th}|_{out}}. \quad (26)$$

The overall thermal resistance seen by the probe reflects two main channels of heat exchange between the probe and its surroundings: the first one is connected with convective cooling by air, the second channel is a heat flux through the probe-sample contact. The latter depends on a thermal resistance of the probe and constriction thermal resistance of

the sample. It leads to the following expression for R_{th}:[22]

$$R_{th}^{-1} = h + \left(R_{thP} + \frac{1}{4\kappa r} \right)^{-1}, \quad (27)$$

where h is the effective heat transfer coefficient describing convective cooling, R_{thP} is the probe thermal resistance to the heat flux from the heat source to the probe sample contact, κ is the thermal conductivity of the sample, and r is the radius of the probe-sample contact.

Measurements were carried out for 5 samples with well-defined thermal conductivity in a range from 1.0 W m^{-1} K^{-1} (BK7 glass) to 490 W m^{-1} K^{-1} (SiC single crystal). The KNT-SThM-1an thermal probe was used. The probe current was the sum of 1.50 mA dc component and the ac component at 320 Hz with amplitude of 0.075 mA. The U_{dc} and $U_{1,rms}$ were measured for the probe being in contact with the sample and the probe lifted 2.0 mm above the sample surface. Each measurement was repeated 20 times and then the mean value and its standard deviation were calculated. Finally R_s and R_d were determined. The phase shift between the ac probe voltage and the ac component of driving current was also recorded.

Results of measurements are shown in Fig. 7. As expected R_d of the probe is larger than R_s. Changes of both resistances caused by different samples are very small. A decrease of R_d with increasing κ of the sample can be noticed, however in some cases this effect is masked by instability of ambient temperature. For R_s any reasonable dependence is not observed. Only the phase is well correlated with the thermal conductivity of samples.

The influence of sample thermal conductivity is much better pronounced for the ratio of $R_d - R_s$ differences calculated for the probe in contact and out of contact with the sample (Fig. 8). The correlation between this quantity and κ is clearly seen. Also the respective signal phase difference exhibits clear dependence on κ of sample. The improvement observed in Fig. 8 compared to Fig. 7 can be understood in terms of sensitivity of signal amplitude to R_{th} which is 0.05 for R_s, 0.15 for R_d, and 1.00 for $R_d - R_s$. The latter value is due to the fact that the difference $R_d - R_s$ is directly proportional to R_{th} (see Eq. (25)). On the other hand, direct comparison

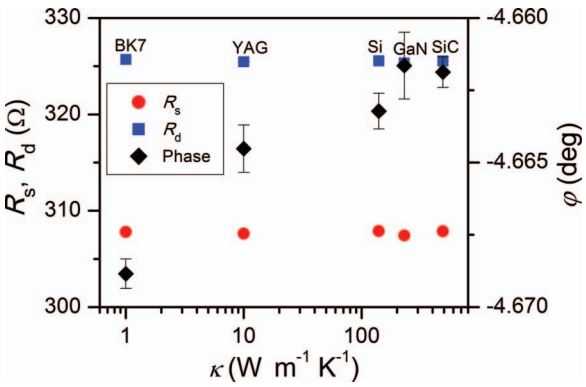

FIG. 7. Static R_s and dynamic R_d resistances of the KNT-SThM-1an probe measured for the probe being in contact with different reference samples. The phase φ of the 1st harmonic of probe voltage is also shown. Detailed description of the experiment is in the text.

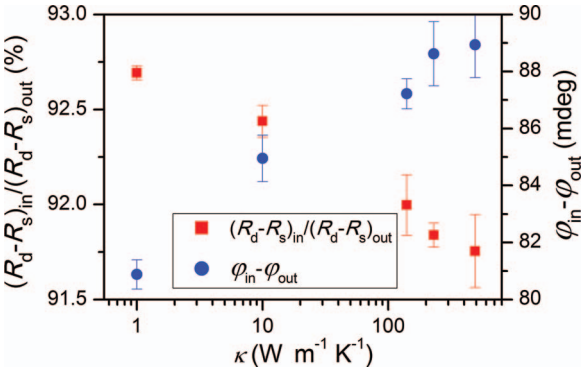

FIG. 8. Ratio defined by Eq. (27) as the function of sample thermal conductivity. The phase difference between the signals measured in and out of contact is also shown.

between amplitude and phase sensitivity is not meaningful. Amplitude sensitivity is dimensionless while phase sensitivity has dimension of degrees. The former has a baseline (origin at zero) while the latter represents a variation of phase angle and it has no baseline (no origin).

The proposed method of thermal measurement by the use of resistive thermal probe was also applied for thermal imaging. As in the previous case the nanofabricated TP was used. The experiment was carried out for a sample with material structures fabricated by through-silicon via (TSV) technology. In this technology vertical electrical connections between stacked integrated circuits are created through the body of chips. The examined sample was a test sample containing TSV structures in silicon. The electrical connections were 4 μm diameter cylinders made of Cu based conductive paste. An atomic force microscopy image of such a connection is shown in Fig. 9.

Detailed description of TSV fabrication process and its structure can be found in Refs. 23 and 24.

It can be expected that the conductive area has higher thermal conductivity than silicon. Results of scanning thermal imaging of the same area are shown in Fig. 10. The imaging was carried out by two modes: the 3ω method at 500 Hz (left column), and the proposed dc + ac method at 500 Hz and 10 kHz (central and right columns, respectively). In the first case the current amplitude was 1.8 mA, while in the dc + ac method the probe was driven by 1.7 mA dc current with 5% ac modulation. All thermal images were recorded at

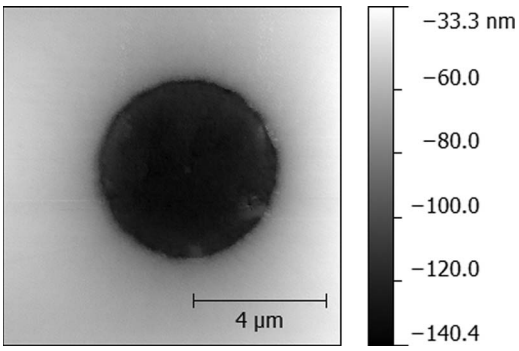

FIG. 9. Topography of silicon wafer containing TSV structure.

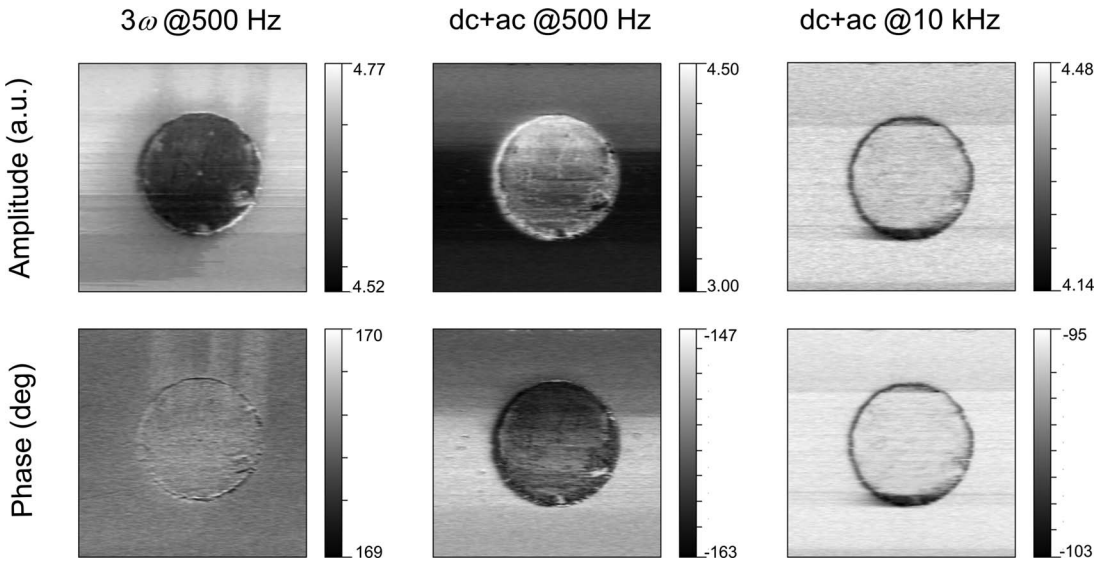

FIG. 10. Amplitude and phase images of TSV structure in silicon obtained by the 3ω method at 500 Hz, and the ac + dc driven probe at 500 Hz (isothermal mode) and at 10 kHz (adiabatic mode). Note the larger dynamic range of both, amplitude and phase, in the isothermal mode.

0.2 Hz scan rate and with 10 ms time constant of the lock-in amplifier.

In amplitude images obtained by both mentioned methods at 500 Hz (the isothermal region) the conductive area is clearly visible; however, signal changes are higher for the dc + ac method. This area is also well pronounced in the dc + ac phase image, while a contrast between silicon and conductive regions in the 3ω phase image is rather low. The images obtained by the dc + ac method at 10 kHz (intermediate region) show only the boundary between regions with different thermal conductivities.

As it was mentioned earlier the lock-in amplifier needs longer time constant when higher harmonics are measured. It can cause signal averaging in the case of scanning measurements. More detailed analysis of amplitude images in left and central columns in Fig. 10 can lead to a conclusion that the image obtained by the dc + ac method is sharper. To confirm this observation signal profiles along the TSV diameter were extracted and compared (Fig. 11).

It can be seen that the dc + ac profile exhibits sharper structures, especially in the vicinity of the TSV boundary. It confirms the conclusion that the spatial resolution of thermal images obtained by the dc + ac method is better than the one of the 3ω method I the same experimental conditions.

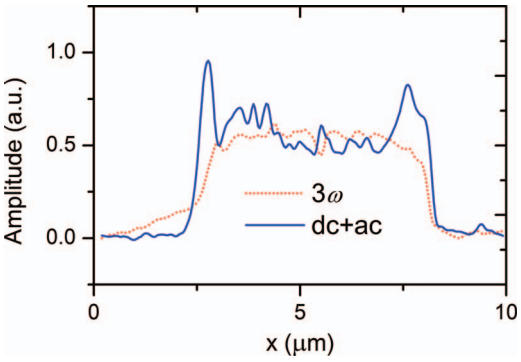

FIG. 11. Profiles of the signal amplitude measured along the TSV region diameter by the 3ω (dotted line) and the dc + ac (solid line) methods. The 3ω profile was inverted and both profiles were rescaled for comparison.

V. CONCLUSIONS

The analysis carried out in this work showed that simultaneous measurements of static (R_s) and dynamic (R_d) TP resistances in SThM experiments can be useful for further data analysis. R_d is approximately 3 times more sensitive to the changes of effective heat abstraction form the TP than R_s. Additionally, taking advantage of lock-in acquisition of ac signals, higher sensitivity and signal-to-noise ratio can be achieved. Measuring R_d on the 1st harmonic requires shorter averaging time for the lock-in output filter (lower time constant) than higher harmonics need. Therefore using signal processing based on R_d rather than on R_s is a good choice in all SThM experiments. However, the greatest benefit of using both resistances is in quantitative thermal measurements. Calculating the $R_d - R_s$ difference increases the sensitivity to the thermal resistance R_{th} to maximum value of 1. The 2nd and the 3rd harmonics have the same sensitivity to R_{th}, but their amplitudes are much lower, therefore uncertainties of measurement are higher. The ratio $R_d - R_s$ values for the TP being in contact with the sample and in air, measured at low frequency limit, is equal to the ratio of effective thermal resistances to the heat flux from the probe to surroundings in these cases. This ratio is clearly correlated with the thermal conductivity of the sample. Experimental determination of R_d requires the TP to be driven with the sum of dc current and small ac current superimposed on it. The ac component (1ω) of the probe voltage at the ac current frequency is measured. Its amplitude is proportional to R_d. Simultaneously the phase of this component can be also determined. It was shown that this phase is also sensitive to the sample thermal conductivity.

It is also shown that the proposed method can be used for thermal imaging. When compared to the thermal imaging

based on the 3ω method, it assures better spatial resolution and better sensitivity to the thermal conductivity of the sample. The best quality images can be obtained in the isothermal region.

Supplemental benefit of proposed method is that the TP is heated mostly by dc current and periodic thermoelastic bending of the probe is reduced. This simplifies approaching the sample and keeping stable probe-sample contact.

ACKNOWLEDGMENTS

This work was supported by the Polish National Centre of Research – NCN, grant N N505 485040 through the Silesian University of Technology, Institute of Physics. Jerzy Bodzenta acknowledges financial support of the Region Champagne Ardenne, France, Contract No. E201202942/2012. Justyna Juszczyk acknowledges a scholarship within the SWIFT POKL.08.02.01-24-005/10 Project co-financed by the European Union under the European Social Fund.

[1]C. C. Williams and H. K. Wickramasinghe, Appl. Phys. Lett. **49**, 1587 (1986).
[2]C. C. Williams and H. K. Wickramasinghe, *1986 IEEE Ultrasonics Symposium Proceedings* (IEEE, New York, 1986) p. 393.
[3]L. Shi and A. Majumdar, J. Heat Transfer **124**, 329 (2002).
[4]F. Menges, H. Riel, A. Stemmer, and B. Gotsmann, Nano Lett. **12**, 596 (2012).
[5]A. Altes, K. Mutamba, R. Heiderhoff, H. L. Hartnagel, and L. J. Balk, Superlattices Microstruct. **35**, 465 (2004).
[6]P. Janus, D. Szmigiel, M. Weisheit, G. Wielgoszewski, Y. Ritz, P. Grabiec, M. Hecker, T. Gotszalk, P. Sulecki, and E. Zschech, Microelectron. Eng. **87**, 1370 (2010).
[7]E. Puyoo, S. Grauby, J.-M. Rampnoux, E. Rouviére, and S. Dilhaire, Rev. Sci. Instrum. **81**, 073701 (2010).
[8]S. Gomes, H. Trannoy, P. Grossel, F. Depasse, C. Bainier, and D. Charraut, Int. J. Therm. Sci. **40**, 949 (2001).
[9]S. Lefèvre and S. Volz, Rev. Sci. Instrum. **76**, 033701 (2005).
[10]M. Chirtoc, J. S. Antoniow, J. F. Henry, P. Dole, and J. Pelzl, in *Advanced Techniques and Applications on Scanning Probe Microscopy*, edited by J. L. Bubendorff and F. H. Lei (Transworld Research Network, Trivandrum, Kerala, 2008), Chap. 10, pp. 197–247.
[11]E. Puyoo, S. Grauby, J.-M. Rampnoux, E. Rouviére, and S. Dilhaire, J. Appl. Phys. **109**, 024302 (2011).
[12]S. Lefèvre, S. Volz, J.-B. Saulnier, C. Fuentes, and N. Trannoy, Rev. Sci. Instrum. **74**, 2418 (2003).
[13]L. David, S. Gomés, P. Galland, B. Vassort, and M. Raynaud, *Proceedings of the 7th European Conference on Thermophysical Properties*, Paper 87, Bratislava, 2005.
[14]S. Gomès, L. David, V. Lysenko, A. Descamps, T. Nychyporuk, and M. Raynaud, J. Phys. D: Appl. Phys. **40**, 6677 (2007).
[15]Y. Zhang, E. E. Castillo, R. J. Mehta, G. Ramanath, and T. Borca-Tasciuc, Rev. Sci. Instrum. **82**, 024902 (2011).
[16]F. A. Guo, K. Y. Zhu, M. Trannoy, and J. Lu, Thermochim. Acta **419**, 239 (2004).
[17]D. G. Cahill, Rev. Sci. Instrum. **61**, 802 (1990).
[18]M. Chirtoc, X. Filip, J. F. Henry, J. S. Antoniow, I. Chirtoc, D. Dietzel, R. Meckenstock, and J. Pelzl, Superlattices Microstruct. **35**, 305 (2004).
[19]J. Gibkes, M. Chirtoc, J. S. Antoniow, R. Wernhardt, and J. Pelzl, Eur. Phys. J. Spec. Top. **153**, 151 (2008).
[20]M. Chirtoc, J. Gibkes, R. Wernhardt, J. Pelzl, and A. Wieck, Rev. Sci. Instrum. **79**, 093703 (2008).
[21]C. Dames and G. Chen, Rev. Sci. Instrum. **76**, 124902 (2005).
[22]J. Juszczyk, M. Wojtol, and J. Bodzenta, Int. J. Thermophys. **34**, 620 (2013).
[23]M. Motoyoshi, Proc. IEEE **97**, 43 (2009).
[24]M. Koyanagi, T. Fukushima, and T. Tanaka, Proc. IEEE **97**, 49 (2009).